2014

An Isolated Multiport DC–DC Converter for Simultaneous Power Management of Multiple Different Renewable Energy Sources

Jianwu Zeng
University of Nebraska-Lincoln, jzeng@huskers.unl.edu

Wei Qiao
University of Nebraska–Lincoln, wqiao@engr.unl.edu

Liyan Qu
University of Nebraska-Lincoln, lqu2@unl.edu

Yanping Jiao
University of Nebraska-Lincoln, yanping.jiao@unl.edu

Pages: 70 - 78, DOI: 10.1109/JESTPE.2013.2293331

An Isolated Multiport DC–DC Converter for Simultaneous Power Management of Multiple Different Renewable Energy Sources

Jianwu Zeng, *Student Member, IEEE*, Wei Qiao, *Senior Member, IEEE*, Liyan Qu, *Member, IEEE*, and Yanping Jiao, *Student Member, IEEE*

***Abstract*— This paper proposes a new isolated multiport dc–dc converter for simultaneous power management of multiple renewable energy sources, which can be of different types and capacities. The proposed dc–dc converter only uses one controllable switch in each port to which a source is connected. Therefore, it has the advantages of simple topology and minimum number of power switches. A general topology of the proposed converter is first introduced. Its principle and operation are then analyzed. The proposed converter is applied for simultaneous maximum power point tracking (MPPT) control of a wind/solar hybrid generation system consisting of one wind turbine generator (WTG) and two different photovoltaic (PV) panels. The experimental results are provided to validate the effectiveness of using the proposed converter to achieve MPPT simultaneously for the WTG and both PV panels.**

***Index Terms*— Isolated dc–dc converter, maximum power point tracking (MPPT), multiport converter, power management, renewable energy, solar energy, wind energy.**

I. Introduction

In RECENT years, there has been a growing interest in generating electricity from distributed renewable energy sources. In many applications, it is required to connect multiple renewable energy sources of different types (e.g., wind and solar) and capacities to a power grid or load [1]–[6]. To perform efficient power management and grid integration for the multiple sources, multiport dc–dc converters have been proposed [5]–[10]. Fig. 1 shows a two-stage, grid-connected multisource renewable energy system, which consists of an isolated multiport dc–dc converter and an inverter [11]. The isolated dc–dc converter has multiple input ports for connecting different sources, such as photovoltaic (PV) panels, wind turbine generators (WTGs), fuel cells, and so on. The multiport dc–dc converter not only regulates the low-level dc voltages of the sources to a constant high level required by the inverter, but also can provide other important control functions, such as maximum power point tracking (MPPT), for the renewable energy sources.

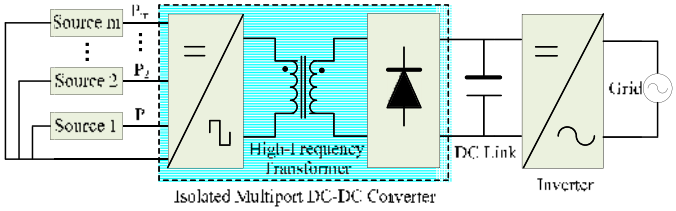

Fig. 1. Configuration of a two-stage, grid-connected, multisource energy system.

There are two categories of integrated isolated multiport converters. One category of converters uses a transformer with a separate winding for each port. Therefore, all ports are electrically isolated [12]–[17]. The other category of converters has multiple ports connected to a single winding on the primary side of a transformer [18]–[25], as shown in Fig. 1. It requires a common ground point for all the input sources. The second topology is preferable due to the advantage of using less number of windings in the transformer.

A number of isolated multiport converters belonging to the second category have been proposed. A widely used topology is the isolated half-bridge converter [7], which used $2m + 2$ controllable switches, where $m(m \geq 2)$ is the number of input ports. Thereafter, in this paper, controllable switches are also called switches. The number of switches was reduced to $2m$ by either using one source as the dc link [21], [22] or reducing switches on the secondary side of the transformer [25]. Recently, a multiport converter topology with $m + 3$ power switches has been proposed [5]. When $m > 3$, this multiport converter has the least number of switches among the existing topologies.

This paper proposes a new isolated multiport dc–dc converter for simultaneous power management of multiple renewable energy sources [26], where only one switch is used in each input port connected to a source. Similar to the converter in [25], the proposed converter does not use any controllable switch on the secondary side of the transformer. Com-

Manuscript received June 1, 2013; revised October 14, 2013 and November 22, 2013; accepted November 23, 2013. Date of publication November 28, 2013; date of current version January 29, 2014. This work was supported by the U.S. Federal Highway Administration under Agreement DTFH61-10-H-00003. Any opinions, findings, and conclusions or recommendations expressed in this publication are those of the authors and do not necessarily reflect the view of the Federal Highway Administration. Recommended for publication by Associate Editor W. Gao.

The authors are with the Power and Energy Systems Laboratory, Department of Electrical Engineering, University of Nebraska-Lincoln, Lincoln, NE 68588-0511 USA (e-mail: jzeng@huskers.unl.edu; wqiao@engr.unl.edu; lqu2@unl.edu; yanping.jiao@unl.edu).

Color versions of one or more of the figures in this paper are available online at http://ieeexplore.ieee.org.

Digital Object Identifier 10.1109/JESTPE.2013.2293331

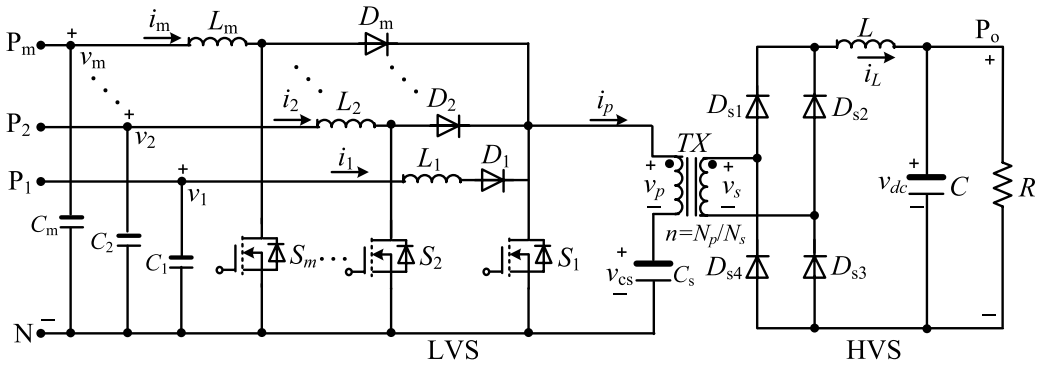

Fig. 2. Topology of the proposed isolated multiport dc–dc converter.

pared with the existing multiport dc–dc converter topologies [18]–[25], the proposed converter has the least number of switches and thereby a lower cost.

The proposed converter is applied for power management of a wind/solar hybrid generation system, which consists of a WTG and two different PV panels. Using a suitably designed perturbation and observation (P&O) MPPT algorithm, the WTG and PV panels can be controlled simultaneously to extract the maximum power from wind and sunlight, respectively, using the proposed converter.

This paper is organized as follows. The topology of the converter is introduced and the operating principle of the converter is analyzed in Section II. Section III discusses the design considerations for the proposed converter. In Section IV, the proposed converter is applied for simultaneous power management of a wind/solar hybrid generation system. The experimental studies are carried out in Section V to testify the effectiveness of the proposed isolated multiport dc–dc converter for simultaneous MPPT control of the wind/solar hybrid generation system. Section VI summarizes this paper with some concluding remarks.

II. Proposed Isolated Multiport DC–DC Converter

Fig. 2 shows the circuit diagram of the proposed isolated multiport dc–dc converter. It consists of a low-voltage-side (LVS) circuit and a high-voltage-side (HVS) circuit connected by a high-frequency transformer TX. The LVS circuit consists of m ports in parallel, one energy storage capacitor C_s, and the primary winding of the transformer. Each port contains a controllable power switch, a power diode, and an inductor. The HVS circuit consists of the secondary winding of the transformer connected to a full-bridge diode rectifier, and a low-frequency LC filter. The transformer's turn ratio is defined as $n = N_p/N_s$, where N_p and N_s are the numbers of turns of the primary and secondary windings, respectively.

This converter has three operating modes: 1) all switches are on; 2) switch S_1 is off while at least one of the other switches is on; and 3) all switches are off. The equivalent circuits of the converter in the three operating modes are shown in Fig. 3. Fig. 4 shows the steady-state waveforms of the converter in

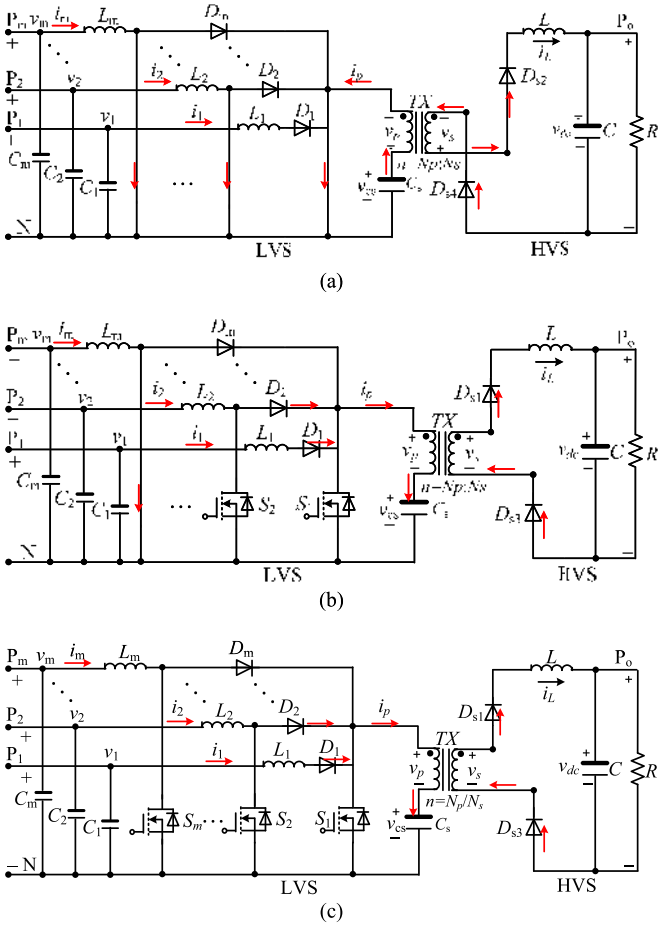

Fig. 3. Equivalent circuits of the three operating modes of the proposed converter. (a) Mode 1: all switches are on. (b) Mode 2: S_1 is off and at least one of the other switches is on. (c) Mode 3: all switches are off.

one switching period covering the three operating modes when $m = 3$. To facilitate the explanation of the converter operation, the state-space equations for different modes are written in the following form:

$$M \cdot \dot{X} = A \cdot X + B \tag{1}$$

where $M = \text{diag}(L_1, L_2, \ldots, L_m, C_s, L, C)$ is a $(m+3) \times (m+3)$ diagonal matrix, $X = [i_1, i_2, \ldots, i_m, v_{\text{cs}}, i_L, v_{\text{dc}}]^T$ is

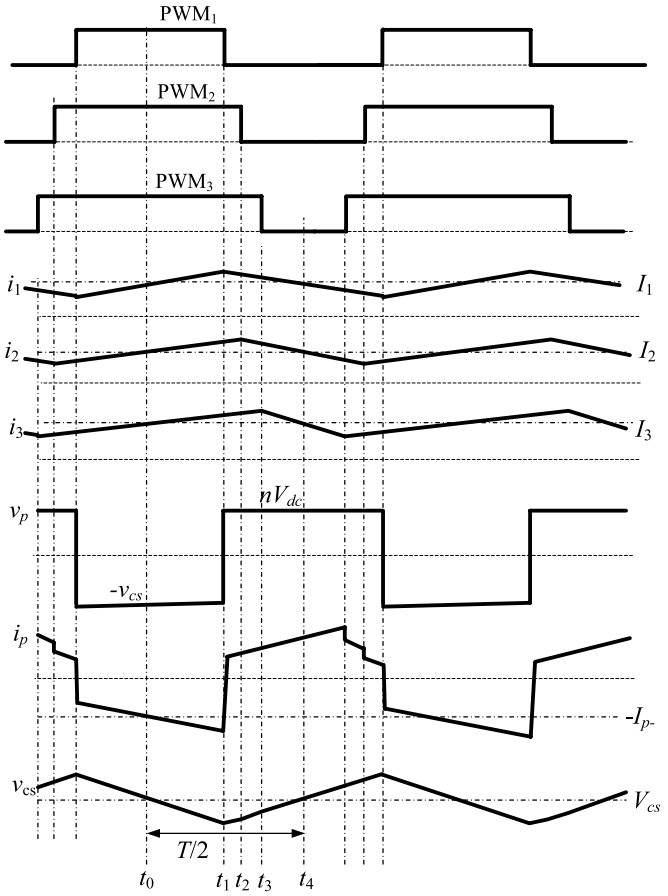

Fig. 4. Waveforms of the proposed converter when $m = 3$.

a $(m + 3) \times 1$ state vector, A is the $(m + 3) \times (m + 3)$ coefficient matrix, and B is a $(m + 3) \times 1$ vector containing input signals and some state variables.

Mode 1: $t \in [t_0, t_1]$ (see Fig. 4), during which all of the switches are on and the inductors $L_1, \ldots, L_m$ store the energy extracted from the sources; while the energy stored in the capacitor C_s in the previous switching cycle is delivered to the HVS through the diodes D_{s2} and D_{s4}. The state-space equations can be described as follows:

$$M \cdot \dot{X} = \begin{bmatrix} 0 & 0 & \cdots & 0 & 0 & 0 & 0 \\ 0 & 0 & \cdots & 0 & 0 & 0 & 0 \\ \vdots & \vdots & \ddots & \vdots & \vdots & \vdots & \vdots \\ 0 & 0 & \cdots & 0 & 0 & 0 & 0 \\ 0 & 0 & \cdots & 0 & 0 & 0 & 0 \\ 0 & 0 & \cdots & 0 & 1/n & 0 & -1 \\ 0 & 0 & \cdots & 0 & 0 & 1 & -1/R \end{bmatrix} \cdot X + \begin{bmatrix} v_1 \\ v_2 \\ \vdots \\ v_m \\ -i_p \\ 0 \\ 0 \end{bmatrix} \quad (2)$$

Mode 2: $t \in [t_1, t_3]$, during which S_1 is off and at least one switch S_k ($k = 2, \ldots,$ or m) is on. Actually, there are $2^{m-1}-1$ different scenarios in this mode depending on the states of the other $(m - 2)$ switches $S_2, \ldots, S_{k-1}, S_{k+1}, \ldots, S_m$. One scenario is illustrated as an example, in which only one switch S_k is on and all other switches are off. The state-space equations are

$$M \cdot \dot{X} = \begin{bmatrix} 0 \cdots 0 & 0 & 0 \cdots 0 & -1 & 0 & 0 \\ \vdots \ddots \vdots & \vdots & \vdots \ddots \vdots & \vdots & \vdots & \vdots \\ 0 \cdots 0 & 0 & 0 \cdots 0 & -1 & 0 & 0 \\ 0 \cdots 0 & 0 & 0 \cdots 0 & 0 & 0 & 0 \\ 0 \cdots 0 & 0 & 0 \cdots 0 & -1 & 0 & 0 \\ \vdots \ddots \vdots & \vdots & \vdots \ddots \vdots & \vdots & \vdots & \vdots \\ 0 \cdots 0 & 0 & 0 \cdots 0 & -1 & 0 & 0 \\ 1 \cdots 1 & 0 & 1 \cdots 1 & 0 & 0 & 0 \\ 0 \cdots 0 & 0 & 0 \cdots 0 & 0 & 0 & -1 \\ 0 \cdots 0 & 0 & 0 \cdots 0 & 0 & 1 & -1/R \end{bmatrix} \cdot X + \begin{bmatrix} v_1 - v_p \\ \vdots \\ v_{k-1} - v_p \\ v_k \\ v_{k+1} - v_p \\ \vdots \\ v_m \\ 0 \\ v_p/n \\ 0 \end{bmatrix} \quad (3)$$

Mode 3: $t \in [t_3, t_4]$, during which all switches are off. The state-space equations are

$$M \cdot \dot{X} = \begin{bmatrix} 0 & 0 \cdots 0 & -1 & 0 & 0 \\ 0 & 0 \cdots 0 & -1 & 0 & 0 \\ \vdots & \vdots \ddots \vdots & \vdots & \vdots & \vdots \\ 0 & 0 \cdots 0 & -1 & 0 & 0 \\ 1 & 1 \cdots 1 & 0 & 0 & 0 \\ 0 & 0 \cdots 0 & 0 & 0 & -1 \\ 0 & 0 \cdots 0 & 0 & 1 & -1/R \end{bmatrix} \cdot X + \begin{bmatrix} v_1 - v_p \\ v_2 - v_p \\ \vdots \\ v_m - v_p \\ 0 \\ v_p/n \\ 0 \end{bmatrix} \quad (4)$$

With (2)–(4), the average state-space model can be derived as follows:

$$M \cdot \dot{X} = \begin{bmatrix} 0 & 0 & \cdots & 0 & -(1-d_1) & 0 & 0 \\ 0 & 0 & \cdots & 0 & -(1-d_2) & 0 & 0 \\ \vdots & \vdots & \ddots & \vdots & \vdots & \vdots & \vdots \\ 0 & 0 & \cdots & 0 & -(1-d_m) & 0 & 0 \\ (1-d_1) & (1-d_2) & \cdots & (1-d_m) & 0 & 0 & 0 \\ 0 & 0 & \cdots & 0 & d_1/n & 0 & 0 \\ 0 & 0 & \cdots & 0 & 0 & 1 & -1/R \end{bmatrix} \cdot X + \begin{bmatrix} v_1 - (1-d_1)v_p \\ v_2 - (1-d_2)v_p \\ \vdots \\ v_m - (1-d_m)v_p \\ -d_1 \cdot i_p \\ (1-d_1) \cdot v_p/n \\ 0 \end{bmatrix} \quad (5)$$

where d_k ($k = 1, \ldots, m$) is the duty cycle of the switch S_k.

The equilibrium points can be calculated by setting all time-derivative terms in (5) to be zero, then

$$D_k = 1 - (1 - D_1) \cdot V_k / V_1 \quad k = 2, \ldots, m \quad (6)$$

$$I_{p-} \cdot D_1 = \sum_{k=1}^{m} I_k (1 - D_k) \quad (7)$$

where D_k represents the steady-state value of d_k and V_k is the steady-state voltage of the kth input port of the converter. Equation (7) shows the power conservation law in the capacitor C_s, where I_{p-}, as shown in Fig. 4, is the mean absolute value of i_p when S_1 is on, and I_k is the steady-state values of i_k.

III. Design Considerations

To make multiple sources work effectively, the following requirement should be satisfied: the switch S_k $(k = 2, \ldots, m)$ should not be turned off before S_1 is switched off; otherwise, L_k will continuously store energy through S_1 even S_k is off, which is not desired. To meet this requirement, the following inequality should be satisfied for the converter

$$\min\{d_2,\ d_3, \ldots,\ d_m\} \geq d_1 \tag{8}$$

Inequality (8) is met if the input voltage of Port 1 (P_1) is the largest, namely the following inequality is satisfied:

$$V_1 \geq \max\{V_2, V_3, \ldots, V_m\} \tag{9}$$

where V_k is the output voltage of the kth source $(k = 1, \ldots, m)$. In practice, the renewable energy source with the largest nominal output voltage will be connected to Port 1. A violation of (9) may lead to one of the following two scenarios.

Scenario 1 *($V_1 = 0$):* If no power is available from Port 1, (9) is no longer valid but (8) should still be satisfied. In this scenario, the duty cycle of the switch S_1 is set to be a constant value such that (8) is satisfied, e.g., $d_1 = 0.4$, and the function of the switch S_1 is to change the direction of the current i_p flowing through the transformer. Specifically, when S_1 is off, the current i_p flows from the other sources to the transformer to charge the capacitor C_s. When S_1 is on, the capacitor C_s discharges so that the direction of the current i_p reverses.

Scenario 2 *($0 < V_1 < \max\{V_2, V_3, \ldots, V_m\}$):* If the maximum power that can be generated by the renewable energy source at Port 1 is low such that (9) cannot be satisfied, (8) should still be satisfied. In this scenario, the duty cycle of the switch S_1 will be increased to a predefined maximum value (e.g., 0.4) by the MPPT controller such that (8) is satisfied, and the function of the switch S_1 is the same as that in Scenario 1. In this scenario, the power generated by the renewable energy source connected to Port 1 might be less than the maximum power that can be generated by the source. However, the difference between the generated and the maximum power at Port 1 is small because the maximum available power at Port 1 is usually very low in this scenario.

It should be noted that in the aforementioned two scenarios, the sources connected to other ports (i.e., Ports 2–m) can still be controlled simultaneously and independently in the MPPT mode by appropriately controlling the duty cycles of the corresponding switches. Therefore, in Scenario 1, the power management of all the ports is still independent. In Scenario 2, the power management of Port 1 is not independent, which slightly affects the power generated from Port 1. However, Scenario 2 can be avoided by connecting a boost type voltage regulator between the source and Port 1 [27] so that (9) is always satisfied.

The parameters of the components of the converter need to be properly designed. These include the transformer turn ratio n, inductances L_k $(k = 1, \ldots, m)$ and L, capacitances C_k $(k = 1, \ldots, m)$ and C_S, and the switches S_k $(k = 1, \ldots, m)$. The turn ratio of the transformer is designed based on the output voltage $V_{\rm dc}$ and the source voltage V_1 of Port 1 [27]

$$n = 2 \cdot V_1 \cdot D_1 / V_{\rm dc}. \tag{10}$$

The design of the inductance L_k $(k = 1, \ldots, m)$ is the same as that in the dc–dc boost converter. When S_k is on, the voltage across the inductor L_k is V_k, then

$$V_k = L_k \frac{\Delta I_k}{D_k \cdot T_s} \qquad k = 1, 2, \ldots, m \tag{11}$$

where ΔI_k is the desired current ripple of the inductor L_k and T_s is the switching period. Therefore, the inductance can be calculated by the following formula:

$$L_k = \frac{V_k \cdot D_k}{f_s \cdot \Delta I_k} \qquad k = 1, 2, \ldots, m \tag{12}$$

where f_s is the switching frequency of the converter. When S_1 is on, the voltage across the secondary inductor L is $V_1/n - V_{\rm dc}$, and therefore

$$L = \frac{(V_1/n - V_{\rm dc}) \cdot D_1 \cdot T_s}{\Delta I_L} = \frac{V_1 \cdot (1 - 2D_1) \cdot D_1}{f_s \cdot n \cdot \Delta I_L} \tag{13}$$

where ΔI_L is the desired current ripple of the inductor L. Particularly, when $D_1 = 0.25$, L achieves its peak value

$$L_{\max} = \frac{V_1}{8 f_s \cdot n \cdot \Delta I_L}. \tag{14}$$

Then, ΔI_L can be controlled within a certain value if selecting $L > L_{\max}$.

In the steady state, the inductor current equals to the source current in each input port, and the capacitor C_k $(k = 1, \ldots, m)$ provides the ripple current ΔI_k of the inductor

$$\Delta I_k = C_k \frac{\Delta v_k}{D_k \cdot T_s} \qquad k = 1, 2, \ldots, m \tag{15}$$

where Δv_k is the voltage ripple of C_k. Then

$$C_k = \frac{\Delta I_k \cdot D_k}{f_s \cdot \Delta v_k} \qquad k = 1, 2, \ldots, m. \tag{16}$$

Similarly, the capacitor C provides the extra current to balance the ripple current ΔI_L caused by the inductor L. Then, the capacitance C can be calculated from (16) with the use of $\Delta I_k = \Delta I_L$, $D_k = D_1$, and $\Delta v_k = \Delta v_{\rm dc}$.

When S_k is off, the current flowing through C_s is increased by I_k, then the capacitance C_s is determined as follows:

$$C_s = \frac{\sum_{k=1}^{m} I_k(1 - D_k) \cdot T_s}{\Delta v_{\rm cs}} = \frac{\sum_{k=1}^{m} I_k(1 - D_k)}{f_s \cdot \Delta v_{\rm cs}} \tag{17}$$

where $\Delta v_{\rm cs}$ is the voltage ripple of C_s.

The peak voltage of the switch S_k $(k = 2, \ldots, m)$ is $V_k/(1 - D_k)$, which equals to $V_1/(1 - D_1)$ according to (6). The peak current flowing through the switch S_k $(k = 2, \ldots, m)$ is I_k, which is less than that flowing through S_1. When S_1 is on, as shown in Fig. 3(a), the inductor L_1 stores energy and the capacitor C_s discharges, then the current flowing through S_1 becomes

$$I_{S_1} = I_1 + I_{p-} = \frac{I_1 + \sum_{k=2}^{m} I_k(1 - D_k)}{D_1} \tag{18}$$

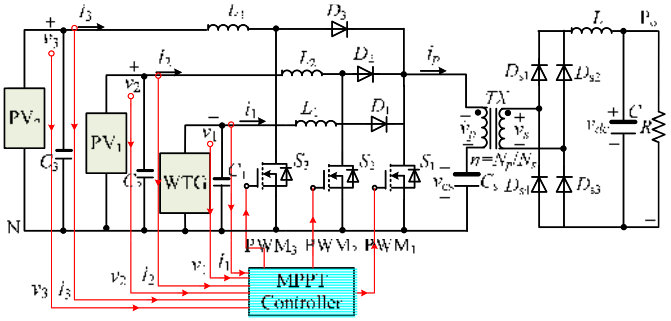

Fig. 5. Signal flows in the wind/solar hybrid generation system managed by the proposed converter.

where I_{S_1} is the maximum drain-to-source current of the switch S_1. Then, the switches are selected based on their peak voltages and maximum currents. In this paper, the allowed maximum voltages and currents of the selected switches are twice their calculated peak values.

IV. Simultaneous Power Management for a Wind/Solar Hybrid Generation System Using the Proposed Converter

Due to voltage variation and voltage sampling error, (6) will not be strictly held if D_k $(k = 2, \ldots, m)$ are fixed. If (6) is not met, the power will be mainly supplied by one port, e.g., Port 1, while the other ports can only supply a little power. This issue is caused by the parallel connected ports, which are coupled with each other [15]. Therefore, a control strategy is required to decouple the power flow management for each port. In this paper, a simple decoupling strategy is proposed, in which only the duty cycle of one switch is being updated at a time. For example, when d_1 is being updated, other duty cycles d_k $(k = 2, \ldots, m)$ are fixed so that the voltage and current in Port 1 can be controlled. The strategy is implemented by setting different updating frequencies for the duty cycles in different ports. For example, the updating frequency of d_k $(k = 1, \ldots, m-1)$ is set lower than that of d_{k+1}. Once the decoupling strategy is determined, the controller for each port can be designed individually.

In this paper, the proposed converter is applied for MPPT control of a wind/solar hybrid generation system consisting of a WTG and two PV panels, as shown in Fig. 5. The MPPT controller uses a P&O MPPT algorithm [28] to maximize the output power of the WTG and two PV panels simultaneously under various weather conditions. Since the wind flow changes more drastically than the solar radiation and the temperature, the updating frequency of d_1 is set to be the highest.

As shown in Fig. 5, the MPPT controller uses the output voltage and current of each source as the input to generate an appropriate pulsewidth modulated signal for the corresponding switch. The flowchart of the P&O MPPT algorithm is shown in Fig. 6, where $V_s(k)$ and $P_s(k)$ are the sampled voltage and power of each source at the kth step, respectively, and Δd is a predefined perturbation value of the switch duty cycle in two consecutive switching periods. The updated duty cycle causes a change in the source current, which leads to the variation of the output power of the source. As shown in Fig. 6, the power

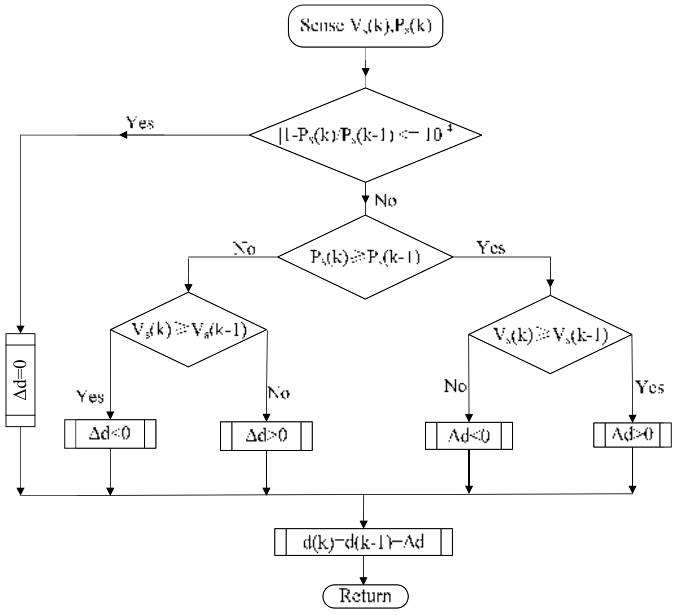

Fig. 6. Flowchart of the P&O MPPT algorithm.

variation and duty cycle perturbation in the previous step are used to determine the direction (i.e., positive or negative) of the duty cycle perturbation in the next step.

To test the MPPT results for the two PV panels and the WTG, it is necessary to obtain the ideal maximum power points (MPPs) of the three sources under various conditions. For a PV panel, the power–voltage (P–V) characteristic curve can be assumed unchanged within every 3-min interval in a clear day. Then, the MPPs can be derived by gradually increasing the duty ratio from a low to a high value. The MPPs of the WTG are calculated using the measured wind speed and other parameters provided by the manufacture as follows:

$$P_{\mathrm{MPP}}(t) = \begin{cases} C_p \cdot \frac{1}{2} \cdot \rho \cdot \pi \cdot r^2 \cdot v_{\mathrm{wind}}^3 & v_{\mathrm{cut\_in}} < v_{\mathrm{wind}} < v_{\mathrm{norm}} \\ P_{\mathrm{norm}} & v_{\mathrm{norm}} \le v_{\mathrm{wind}} < v_{\mathrm{cut\_out}} \\ 0 & v_{\mathrm{wind}} \le v_{\mathrm{cut\_in}},\ v_{\mathrm{wind}} \ge v_{\mathrm{cut\_out}} \end{cases} \tag{19}$$

where P_{MPP} is the maximum power output of the wind turbine, v_{wind} is the wind speed, which can be measured by an anemometer, ρ is the air density, r is the radius of the wind turbine rotor plane, $v_{\mathrm{cut\_in}}$, v_{norm}, and $v_{\mathrm{cut\_out}}$ are the cut-in, nominal, and cut-out wind speeds of the wind turbine, respectively, P_{norm} is the nominal power of the wind turbine and its value is 160 W, and C_p is the power coefficient of the wind turbine. According to Betz' law, the maximum value of C_p is 0.59. According to the power-wind speed characteristic of the wind turbine provided by the manufacture, when the average wind speed is 13.4 m/h, the monthly generated power of this wind turbine is 40 kWh. Therefore, the maximum value of C_p is calculated to be 0.4458 for the wind turbine in this paper.

V. Experimental Results

With the analysis and design guidelines presented in the previous sections, the proposed converter was constructed

Fig. 7. Experimental setup.

TABLE I
COMPONENT SPECIFICATIONS OF THE CONVERTER CONSTRUCTED

L_1	420 μH	$C_1 \sim C_3$	1000 μF
L_2	280 μH	C_S	1000 μF
L_3	300 μH	C	1000 μF
L	1120 μH	n	7:28
S_1	FDP24N40	$S_2 \sim S_3$	FDP3632
$D_1 \sim D_3$	MUR1510	$Ds_1 \sim Ds_4$	EGP50D

in hardware for power management of an actual wind/solar hybrid generation system. Fig. 7 shows the whole system, which consists of the proposed multiport dc–dc converter, three renewable energy sources, a dSPACE 1005 controller board, and a resistive load. The control algorithm was implemented in the dSPACE 1005 real-time control platform. The three sources are a Southwest Windpower Air Breeze WTG with a rated dc output voltage of 48 V, a BP SX 3175 PV panel (PV1) with the voltage and current of 36.1 V and 4.85 A, respectively, at the maximum power output, and a SunWize SW-S110P PV panel (PV2) with the voltage and current of 17.4 V and 6.3 A, respectively, at the maximum power output. The switching frequency and nominal output voltage of the dc–dc converter are 60 kHz and 100 V, respectively. The updating frequency of d_1, d_2, and d_3 are set as 2000, 500, and 100 Hz, respectively. The parameters of the converter prototype used in the experiments are listed in Table I.

A. Steady-State Waveforms

Fig. 8(a) shows the measured waveforms of the currents i_1 and i_2 flowing through the two inductors L_1 and L_2, respectively, where i_1 and i_2 increase when the two switches S_1 and S_2 are switched on; when the two switches are off, i_1 and i_2 decrease.

Fig. 8(b) shows the current waveforms of the two inductors L_2 and L_3, where i_3 is the current flowing through the inductor L_3. i_3 increases when the switch S_3 is switched on and decreases when S_3 is off, which is similar to i_1 and i_2. The mean values of the three source currents in Fig. 8(a) and (b) are $I_1 = 1.41$ A, $I_2 = 3.82$ A, and $I_3 = 3.28$ A, which shows that the three sources WTG, PV1, and PV2 are connected to the multiport dc–dc converter to supply power simultaneously.

Fig. 8(c) shows the waveform of i_p, which is the current flowing through the primary side of the transformer. When S_1 is on, the capacitor C_s discharges since the current is negative; during the period when S_1 is off, the current becomes positive, which charges C_s; when S_2 is off, i_p increases because

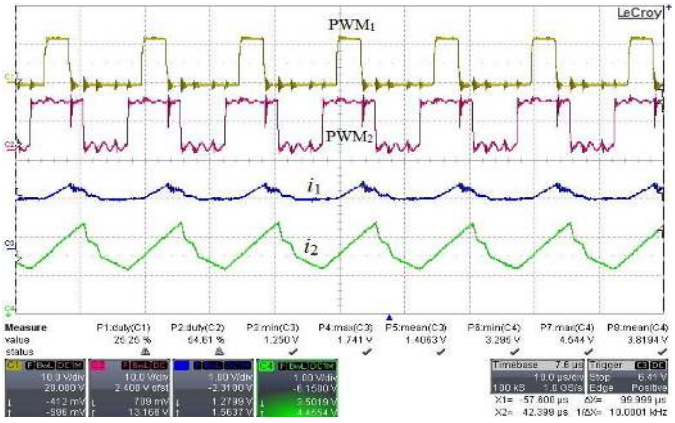

(a)

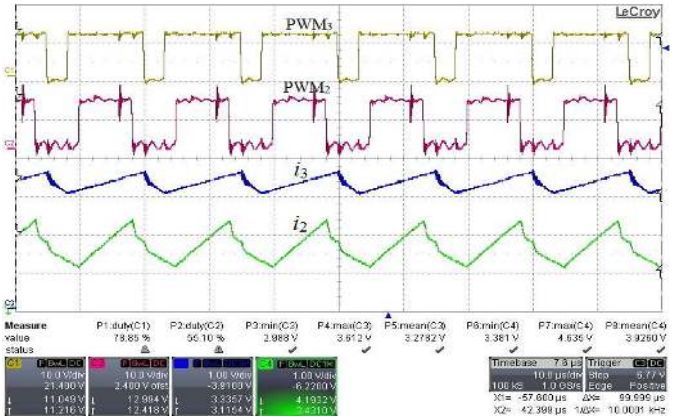

(b)

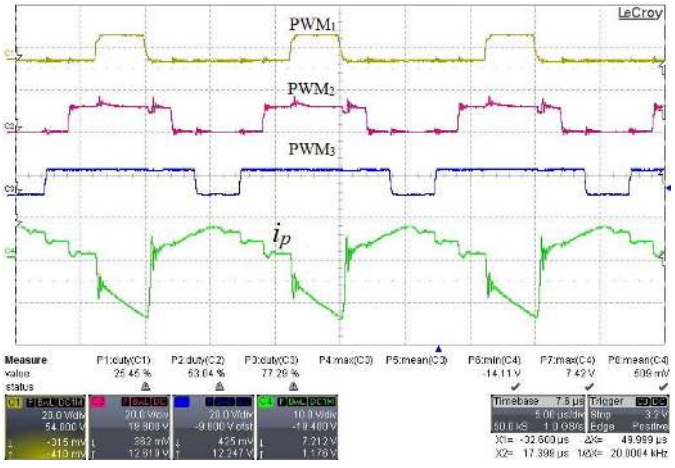

(c)

Fig. 8. Current waveforms of the multiport dc–dc converter. (a) Currents of the two inductors L_1 and L_2 (CH_3 and CH_4: 1 A/div). (b) Currents of the two inductors L_2 and L_3 (CH_3 and CH_4: 1 A/div). (c) Current on the primary side of the transformer (CH_4: 10 A/div).

$i_p = i_1 + i_2$; i_p further increases to $i_1 + i_2 + i_3$ when all of the three switches are off. The waveforms in Fig. 8 are consistent with those in Fig. 4, which validates the theoretical analysis.

B. MPPT Results

Fig. 9 shows the MPPT results of the two PV panels, where the P–V characteristic curves were derived by connecting each of the two PV panels to Port 1 at a time and gradually

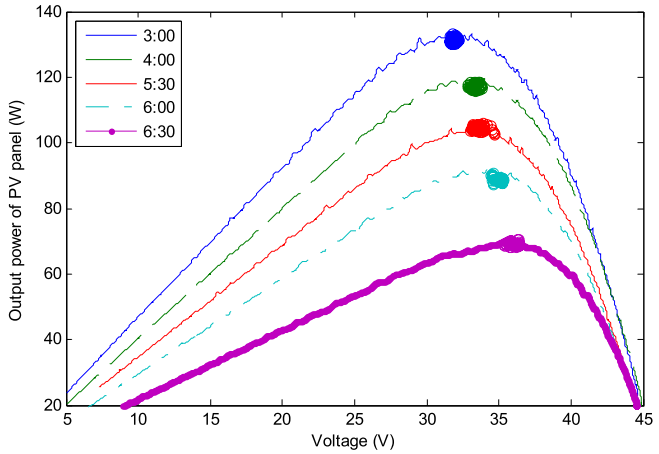

(a)

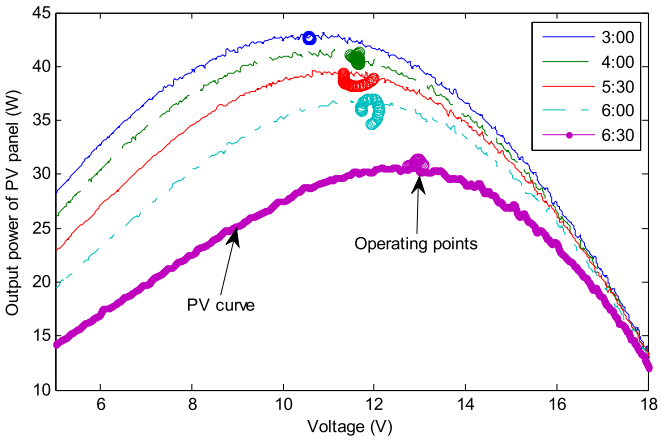

(b)

Fig. 9. MPPT results of the PV panels. (a) PV1. (b) PV2.

increasing the duty cycle of switch S_1 from a low value (0.1) to a high value (0.8) in 15 s, leading to a gradual change of the operating points of the PV panel.

As shown in Fig. 9, the operating points of the two PV panels are close to their respective MPPs, which shows that the proposed multiport dc–dc converter has successfully achieved MPPT control for different PV panels simultaneously. In Fig. 9, the operating points are higher than the ideal MPPs sometimes because there are capacitors connected with the PV panels in parallel for storing energy, and the instantaneous power can be larger than the MPPs. Small oscillations of the operating points are caused by the P&O MPPT algorithm in which the duty ratio varies slightly around the optimal duty ratio from time to time. Such oscillations of power, however, are relatively small compared with the average power value and are acceptable. The results obtained at different times of the day show that the proposed converter and control algorithm regulate the two PV sources correctly to generate the maximum power over the whole day.

Fig. 10 shows the MPPT result of the WTG. As shown in Fig. 10(a), the wind speed measured by the anemometer varies from time to time. The ideal MPP fluctuated with the wind speed. The measured output power of the WTG follows closely the ideal MPPs in Fig. 10(b), which shows the effectiveness of the proposed multiport dc–dc converter and the MPPT algorithm.

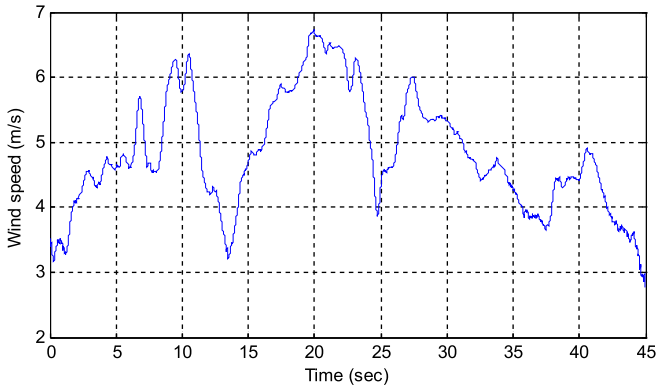

(a)

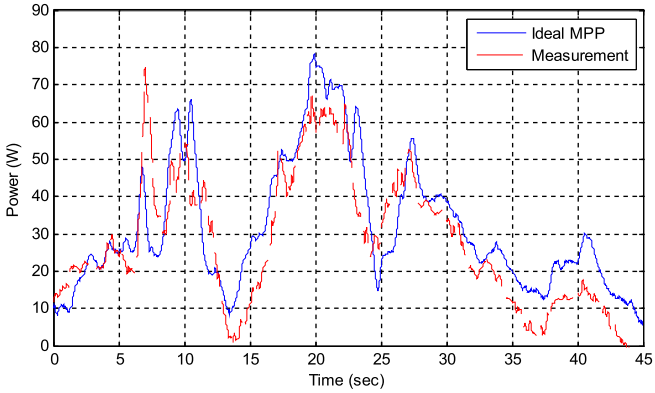

(b)

Fig. 10. Experimental result of WTG. (a) Wind speed profile. (b) MPPT result of the WTG.

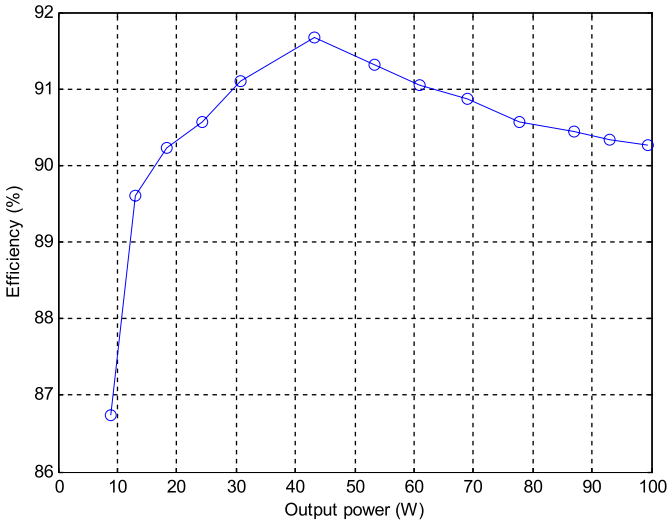

Fig. 11. Measured efficiency with respect to the output power.

C. Efficiency

Three voltage sources were connected to the three input ports of the converter to test its efficiency. During the test, the voltages of the three sources connected to the input ports 1∼3 were set to be 48, 36, and 17.4 V, respectively; the ratio of the input powers among the three input ports 1∼3 were approximately regulated as 1:1:0.6, which is the same as the ratio of the maximum powers of the three sources. Fig. 11 shows the measured efficiency with respect to the

output power of the converter. The efficiency first increases with the increase of the output power. Particularly, when the output power is 43 W, the maximum efficiency reaches 91.7%. Then, the efficiency gradually decreases with the increase of the load but is always higher than 90%.

VI. Conclusion

An isolated multiport dc–dc converter that uses the minimum number of switches has been proposed for simultaneous power management of multiple renewable energy sources. The proposed converter has been applied for simultaneous power management of a three-source wind/solar hybrid generation system. The experimental results have been provided to show the effectiveness of the proposed converter. The advantage of the proposed multiport dc–dc converter is its simple topology while having the capability of MPPT control for different renewable energy sources simultaneously. Moreover, the proposed converter can be easily applied for power management of other types of renewable energy sources.

References

[1] J. Kassakian and T. Jahns, "Evolving and emerging applications of power electronics in systems," *IEEE J. Emerging Sel. Topics Power Electron.*, vol. 1, no. 2, pp. 47–58, Jun. 2013.

[2] O. Lucia, I. Cvetkovic, H. Sarnago, D. Boroyevich, P. Mattavelli, and F. C. Lee, "Design of home appliances for a DC-based nanogrid system: An induction range study case," *IEEE J. Emerging Sel. Topics Power Electron.*, vol. 1, no. 4, pp. 315–326, Dec. 2013.

[3] J. Carr, J. Balda, and A. Mantooth, "A high frequency link multiport converter utility interface for renewable energy resources with integrated energy storage," in *Proc. IEEE Energy Convers. Congr. Exposit.*, Sep. 2010, pp. 3541–3548.

[4] W. Qiao, A. Sharma, J. Hudgins, E. Jones, and L. Rilett, "Wind/solar hybrid generation-based roadway microgrids," in *Proc. IEEE Power Energy Soc. General Meeting*, Jul. 2011, pp. 1–7.

[5] Z. Qian, O. Abdel-Rahman, and I. Batarseh, "An integrated four-port DC/DC converter for renewable energy applications," *IEEE Trans. Power Electron.*, vol. 25, no. 7, pp. 1877–1887, Jul. 2010.

[6] C. Shen and S. Yang, "Multi-input converter with MPPT feature for wind-PV power generation system," *Int. J. Photoenergy*, Article ID 129254, pp. 129254-1–129254-13, Apr. 2013.

[7] H. Tao, A. Kotsopoulos, J. Duarte, and M. Hendrix, "Family of multiport bidirectional DC-DC converters," *IEE Proc. Electr. Power Appl.*, vol. 153, no. 3, pp. 451–458, May 2006.

[8] M. Qiang, Z. Xu, and W. Wu, "A novel multi-port DC-DC converter for hybrid renewable energy distributed generation systems connected to power grid," in *Proc. IEEE Int. Conf. Ind. Technol.*, Apr. 2008, pp. 1–5.

[9] S. Yu and A. Kwasinski, "Analysis of soft-switching isolated time-sharing multiple-input converters for DC distribution systems," *IEEE Trans. Power Electron.*, vol. 28, no. 4, pp. 1783–1794, Apr. 2013.

[10] J. Zeng, W. Qiao, and L. Qu, "An isolated multiport DC-DC converter for simultaneous power management of multiple renewable energy sources," in *Proc. IEEE Energy Convers. Congr. Exposit.*, Sep. 2012, pp. 3741–3748.

[11] Q. Li and P. Wolfs, "A review of the single phase photovoltaic module integrated converter topologies with three different DC link configurations," *IEEE Trans. Power Electron.*, vol. 23, no. 3, pp. 1320–1333, May 2008.

[12] H. Matsuo, T. Shigemizu, F. Kurokawa, and N. Watanabe, "Characteristics of the multiple-input DC-DC converter," *IEEE Trans. Ind. Electron.*, vol. 51, no. 3, pp. 625–631, Jun. 2004.

[13] Y. Chen, Y. Liu, and F. Wu, "Multi-input DC/DC converter based on the multiwinding transformer for renewable energy applications," *IEEE Trans. Ind. Appl.*, vol. 38, no. 4, pp. 1096–1104, Aug. 2002.

[14] X. Sun, G. Pei, S. Yao, and Z. Chen, "A novel multi-port DC/DC converter with bi-directional storage unit," in *Proc. Int. Power Electron. Motion Control Conf.*, Jun. 2012, pp. 1771–1775.

[15] C. Zhao, S. Round, and J. Kolar, "An isolated three-port bidirectional DC-DC converter with decoupled power flow management," *IEEE Trans. Power Electron.*, vol. 23, no. 5, pp. 2443–2453, Sep. 2008.

[16] Z. Zhang, Z. Ouyang, O. Thomsen, and M. Andersen, "Analysis and design of a bidirectional isolated DC-DC converter for fuel cells and supercapacitors hybrid system," *IEEE Trans. Power Electron.*, vol. 27, no. 2, pp. 848–859, Feb. 2012.

[17] D. Liu and H. Li, "A ZVS bi-directional DC-DC converter for multiple energy storage elements," *IEEE Trans. Power Electron.*, vol. 21, no. 5, pp. 1513–1517, Sep. 2006.

[18] Z. Wang and H. Li, "Integrated MPPT and bidirectional battery charger for PV application using one multiphase interleaved three-port DC-DC converter," in *Proc. IEEE Appl. Power Electron. Conf. Exposit.*, Mar. 2011, pp. 295–300.

[19] Z. Wang and H. Li, "An integrated three-port bidirectional DC-DC converter for PV application on a DC distribution system," *IEEE Trans. Power Electron.*, vol. 28, no. 10, pp. 4612–4624, Oct. 2013.

[20] F. Forest, T. Meynard, E. Laboure, B. Gelis, J. Huselstein, and J. Brandelero, "An isolated multicell intercell transformer converter for applications with a high step-up ratio," *IEEE Trans. Power Electron.*, vol. 28, no. 3, pp. 1107–1119, Mar. 2013.

[21] G. Su and F. Peng, "A low cost, triple-voltage bus DC-DC converter for automotive applications," in *Proc. IEEE Appl. Power Electron. Conf. Exposit.*, vol. 2. Mar. 2005, pp. 1015–1021.

[22] Y. Chen, A. Huang, and X. Yu, "A high step-up three-port DC-DC converter for stand-alone PV/battery power systems," *IEEE Trans. Power Electron.*, vol. 28, no. 11, pp. 5049–5062, Nov. 2013.

[23] F. Blaabjerg and K. Ma, "Future on power electronics for wind turbine systems," *IEEE J. Emerging Sel. Topics Power Electron.*, vol. 1, no. 3, pp. 139–152, Sep. 2013.

[24] H. Wu, R. Chen, J. Zhang, Y. Xing, H. Hu, and H. Ge, "A family of three-port half-bridge converters for a stand-alone renewable power system," *IEEE Trans. Power Electron.*, vol. 26, no. 9, pp. 2697–2706, Sep. 2011.

[25] W. Li, J. Xiao, Y. Zhao, and X. He, "PWM plus phase angle shift (PPAS) control scheme for combined multiport DC/DC converters," *IEEE Trans. Power Electron.*, vol. 27, no. 3, pp. 1479–1489, Mar. 2012.

[26] J. Zeng, W. Qiao, and L. Qu, "A single-switch isolated DC-DC converter for photovoltaic system," in *Proc. IEEE Energy Convers. Congr. Exposit.*, Sep. 2012, pp. 3446–3452.

[27] Y. Zhao, C. Wei, Z. Zhang, and W. Qiao, "A review on position/speed sensorless control for permanent-magnet synchronous machine-based wind energy conversion systems," *IEEE J. Emerging Sel. Topics Power Electron.*, vol. 1, no. 4, pp. 203–216, Dec. 2013.

[28] C. Hua, J. Lin, and C. Shen, "Implementation of a DSP-controlled photovoltaic system with peak power tracking," *IEEE Trans. Ind. Electron.*, vol. 45, no. 1, pp. 99–107, Feb. 1998.

Jianwu Zeng (S'10) received the B.Eng. degree in electrical engineering from the Xi'an University of Technology, Xi'an, China, in 2004, and the M.S. degree in control science and engineering from Zhejiang University, Hangzhou, China, in 2006. Currently, he is working toward the Ph.D. degree in electrical engineering with the University of Nebraska-Lincoln, Lincoln, NE, USA.

He joined Eaton Electrical Co., Ltd., Shenzhen, China, in 2006, where he was an Electronic Engineer involved in research and development of soft-switching dc-dc converters for uninterruptible power supply. His current research interests include power electronics, renewable energy, and computational intelligence.

Wei Qiao (S'05–M'08–SM'12) received the B.Eng. and M.Eng. degrees in electrical engineering from Zhejiang University, Hangzhou, China, in 1997 and 2002, respectively, the M.S. degree in high performance computation for engineered systems from Singapore-MIT Alliance, Singapore, in 2003, and the Ph.D. degree in electrical engineering from the Georgia Institute of Technology, Atlanta, GA, USA, in 2008.

He has been with the University of Nebraska-Lincoln, Lincoln, NE, USA, since 2008, where he is currently an Associate Professor with the Department of Electrical Engineering. He is the author or co-author of three book chapters and more than 120 papers in refereed journals and international conference proceedings. His current research interests include renewable energy systems, smart grids, microgrids, condition monitoring and fault diagnosis, energy storage systems, power electronics, electric machines and drives, and computational intelligence for electric power and energy systems.

Dr. Qiao is an Associate Editor of the IEEE TRANSACTIONS ON INDUSTRY APPLICATIONS and the IEEE JOURNAL OF EMERGING AND SELECTED TOPICS IN POWER ELECTRONICS, and the Chair of the Sustainable Energy Sources Technical Thrust of the IEEE Power Electronics Society. He was a recipient of the 2010 National Science Foundation CAREER Award, the 2010 IEEE Industry Applications Society Andrew W. Smith Outstanding Young Member Award, the 2012 UNL College of Engineering Faculty Research and Creative Activity Award, the 2011 UNL Harold and Esther Edgerton Junior Faculty Award, and the 2011 UNL College of Engineering Edgerton Innovation Award. He has received four Best Paper Awards from IEEE IAS, PES, and PELS.

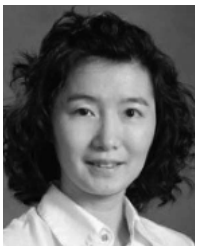

Liyan Qu (S'05–M'08) received the B.Eng. (Hons.) and M.Eng. degrees in electrical engineering from Zhejiang University, Hangzhou, China, in 1999 and 2002, respectively, and the Ph.D. degree in electrical engineering from the University of Illinois at Urbana-Champaign, Urbana, IL, USA, in 2007.

She was an Application Engineer with Ansoft Corporation, Pittsburgh, PA, USA, from 2007 to 2009. She has been with the University of Nebraska-Lincoln, Lincoln, NE, USA, since 2010, where she is currently an Assistant Professor with the Department of Electrical Engineering. Her current research interests include energy efficiency, renewable energy, numerical analysis and computer aided design of electric machinery and power electronic devices, dynamics and control of electric machinery, permanent-magnet machines, and magnetic materials.

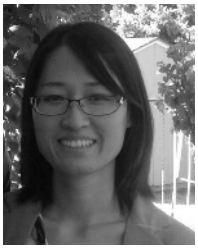

Yanping Jiao (S'10) received the B.Eng. degree in electrical engineering from Tianjin University, Tianjin, China, in 2006, and the Ph.D. degree in electrical engineering from Nanyang Technological University, Singapore, in 2012.

She was a Post-Doctoral Researcher with the Department of Electrical Engineering, University of Nebraska-Lincoln, Lincoln, NE, USA, from 2011 to 2013. Her current research interests include power converters, renewable energy, energy management system, and smart grid.